Contents lists available at SciVerse ScienceDirect

Applied Mathematical Modelling

journal homepage: www.elsevier.com/locate/apm

Analytical estimation of liquid film thickness in two-phase annular flow using electrical resistance measurement

Rongli Wang [a,b], Bo An Lee [a,b], Jeong Seong Lee [a,b], Kyung Youn Kim [c], Sin Kim [a,b,*]

[a] Department of Nuclear and Energy Engineering, Jeju National University, Jeju 690-756, Republic of Korea
[b] Institute for Nuclear Science and Technology, Jeju National University, Jeju 690-756, Republic of Korea
[c] Department of Electronic Engineering, Jeju National University, Jeju 690-756, Republic of Korea

ARTICLE INFO

ABSTRACT

This paper presents an analytical solution to estimate the liquid film thickness in two-phase annular flow through a circular pipe using electrical resistance tomography. Gas–liquid flow with circular gas core surrounded by a liquid film is considered. Conformal mapping is employed to obtain the analytic solution for annular flow with an eccentric circular gas core. The liquid film thickness for an arbitrary annular flow is estimated by comparing the resistance values for concentric and eccentric annular flows. The film thickness estimation has a good performance when the normalized distance between the gas core center and the flow center is less than 0.2 and the void fraction is greater than 0.4, the estimated error of the normalized thickness is less than 0.04.

© 2011 Elsevier Inc. All rights reserved.

1. Introduction

Two-phase flow is commonly encountered in many industrial processes. Due to its practical interest, extensive experimental and theoretical studies were performed to describe two-phase flows in the last decades [1–12]. In the analysis of gas–liquid two-phase flow systems, especially for annular flows, the thickness of liquid film is one of the key parameters. There have been many contributions to develop techniques to measure the thickness of liquid film in the area of two-phase flows. Simulation studies have been conducted to demonstrate the possibility of using a multifiber optic sensor to determine the thickness of a liquid film in a gas–liquid two-phase flow situation by Yu et al. [13]. Schubring et al. [14–16] used planar laser-induced fluorescence to provide direct visualization of the liquid film in upward vertical air–water annular flow, and presented that the film thickness model can be used to estimate the critical liquid flow rate. Kishore and Jayanti [17] developed a finite volume method-based CFD model to simulate annular gas–liquid flow in a duct, and showed that the resulting model gives good predictions of the literature data of annular flow parameters under equilibrium and non-equilibrium conditions.

Of all film thickness measurement techniques, the conductance method is probably most extensively used, which is based on the fact that the liquid and the gas have different conductivity values [18–21]. The parallel wire conductance technique was used to measure the film thickness by Jong and Gabriel [22]. In their work, a pair of wires was stretched across the tube's cross section, drilled through the liquid film and air core, and the electrical conductance between the two wires was

---

* Corresponding author at: Department of Nuclear and Energy Engineering, Jeju National University, Jeju 690-756, Republic of Korea. Tel.: +82 64 754 3647; fax: +82 64 759 9276.
E-mail address: sinkim@jejunu.ac.kr (S. Kim).

measured. That conductance is indicative of the relative proportion of the phases in a particular cross sectional area. Conte and Azzopardi [23] and Geraci and Azzopardi [24] used flush-mounted pin probes and parallel wire conductance technique to collect the liquid film thickness data in their work. The first method was used for very thin films, typically up to 2 mm. Electrodes were pins mounted flush with the pipe surface linked in a circuit to a neighboring, similar electrode. The resistance between a pair of flush-mounted pins was measured and the measurements were converted to film thicknesses using calibration curves. The method is non-intrusive but the response is non-linear. The range of film thickness that can be handled depends on the size and spacing of the electrodes. However, the greater the spacing, the more averaged is the result over the space. Design is based on a compromise between the range of operability and local characteristics of the measurement. The second type, suitable for thicker film thickness, was used only for the bottom side. The parallel wire conductance technique they used was similar to the method employed by Jong and Gabriel [22], with a pair of wires stretched across the tube's cross section and the resistance was measured between the two wires. Fu et al. [25] also reported their work about the measurement of the liquid film thickness by making use of the electrical conductance method. They measured the resistance between two probes placed along the tube. The resistance value depends on the length between the two probes and the area of the conductive liquid according to the definition of the electric resistance. Then the liquid film thickness which is related to the area of the conductive liquid is obtained from the measured resistance. Recently, a review of the film thickness measurement techniques applied to micro-scale two-phase flow system was presented by Tibiriçá et al. [26]. They focused on the recent literature concerning the methods used to measure two-phase liquid film thicknesses in macro- and micro-scale systems.

This work considers the electrical method, specifically the resistance type, using the analytical method to estimate the thickness of water film in two-phase circular annular flow. At first, the two-dimensional potential distribution in the pipe is found analytically using conformal mapping [27–29]. The analytical solutions of the potential distribution for two-region problems for concentric circular case can be determined relatively easily. However, for eccentric case, the computation of the analytical solutions becomes more complicated. Conformal mapping can be used for transforming a given region into a concentric one, thus it is useful to establish a bi-directional link between two geometric frames especially from eccentric circles to concentric circles. From the potential distribution, the resistance is obtained in a series form as a function of the void fraction and the location of the electrode which is also related to the water film thickness. Then the resistance between two electrodes of eccentric case is compared with the resistance value of concentric case to estimate the thickness of water film.

2. Mathematical model

Consider an annular flow composed of water background and circular air core as shown in Fig. 1. σ_w is the conductivity of the water region, u_w the potential distribution of the water region, σ_a the conductivity of the air region and u_a the potential distribution of the air region. The radius of the pipe is a_1 and the radius of the air region is a_2, so the thickness of water film is $T = a_1 - a_2$. Two electrodes are flush-mounted on the inner boundary of the pipe. The width and height of the electrodes are W and H. From Ohm's law, if the voltage between the two electrodes is ΔV and the current applied is I, then the resistance R is $\Delta V/I$. As the first step, we need to obtain the potential distribution in the problem domain to calculate the voltage difference between the two electrodes.

The potential distribution u for a given conductivity σ in the flow domain satisfies the Laplace equation:
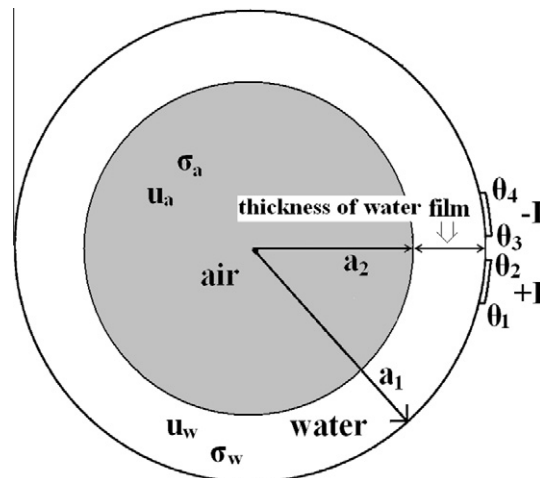
$$\nabla \cdot \sigma \nabla u = 0, \tag{1}$$

Fig. 1. Cross section of the annular flow.

which is subjected to the following boundary and interfacial conditions:

$$\sigma \frac{\partial u}{\partial r}\Big|_{r=a_1} = j(\theta) = \begin{cases} J & \theta \in [\theta_1, \theta_2], \\ -J & \theta \in [\theta_3, \theta_4], \\ 0 & otherwise, \end{cases} \tag{2a}$$

$$u_w(r, \theta)|_{r=a_2} = u_a(r, \theta)|_{r=a_2}, \tag{2b}$$

$$\sigma_w \frac{\partial u_w}{\partial r}\Big|_{r=a_2} = \sigma_a \frac{\partial u_a}{\partial r}\Big|_{r=a_2}, \tag{2c}$$

where $J = I/(WH)$ is the applied current density on the electrode. θ_1, θ_2, θ_3 and θ_4 are the angles of the beginning point and ending point of the two electrodes. As for the gaps between the two electrodes, the proper boundary condition is the insulation condition. In our work, we assumed that the size of the two electrodes is same. Therefore

$$\theta_2 - \theta_1 = \theta_4 - \theta_3 = \Delta\theta = W/R. \tag{3}$$

Practically, the air is non-conductive. Hence, the boundary condition (2b) is not required and (2c) becomes the insulation condition.

2.1. Relationship between resistance and water film thickness for concentric case

The analytical solution of Eq. (1) for concentric case is

$$u_w(r, \theta) = \sum_{n=1}^{\infty} \frac{a_1}{n\sigma_w} \frac{1}{1-\alpha^n} (p_n \cos n\theta + q_n \sin n\theta) \left[\left(\frac{r}{a_1}\right)^n + \alpha^n \left(\frac{r}{a_1}\right)^{-n} \right], \tag{4}$$

where the void fraction of the circular annular flow is defined as

$$\alpha = (a_2/a_1)^2 = ((a_1 - T)/a_1)^2, \tag{5}$$

and the coefficients of Fourier series expansion of the boundary current $j(\theta)$ are

$$p_n = \frac{J}{n\pi} (\sin n\theta_2 - \sin n\theta_1) - \frac{J}{n\pi} (\sin n\theta_4 - \sin n\theta_3), \tag{6}$$

$$q_n = \frac{-J}{n\pi} (\cos n\theta_2 - \cos n\theta_1) + \frac{J}{n\pi} (\cos n\theta_4 - \cos n\theta_3). \tag{7}$$

If we approximate the electrode voltage as the average value over the electrode, then from the analytical solution we can calculate the voltage difference between the two electrodes. On the boundary, $r = a_1$, therefore the resistance between the two electrodes for concentric case becomes

$$R_c = \Delta V/I = \frac{a_1}{\sigma_w I \Delta\theta} \sum_{n=1}^{\infty} \frac{1}{n^2(1-\alpha^n)} \left[(p_n \sin n\theta - q_n \cos n\theta)|_{\theta_1}^{\theta_2} - (p_n \sin n\theta - q_n \cos n\theta)|_{\theta_3}^{\theta_4} \right]. \tag{8}$$

2.2. Relationship between resistance and water film thickness for eccentric case

For eccentric case, we can use the linear fractional conformal mapping [27–29] to transform eccentric circles into concentric circles,

$$w(z) = (z - \beta_1)/(z - \beta_2), \tag{9}$$

where $z = re^{i\theta} = x + iy$ and $w = r'e^{i\theta'} = \tau + i\upsilon$ are both complex numbers. β_1 and β_2 are the coordinates of the two symmetrical points of the circles and are determined by the following equations:

$$\begin{cases} \beta_1\beta_2 = a_1^2, \\ (\beta_1 - L)(\beta_2 - L) = a_2^2, \end{cases} \tag{10}$$

where L is the distance of the center of two eccentric circles.

From the solution of Eq. (10), we can get

$$\begin{cases} \beta_1 = \frac{1}{2L}\left[\left(L^2 + a_1^2 - a_2^2\right) - \sqrt{\left(a_1^2 + a_2^2 - L^2\right)^2 - 4a_1^2 a_2^2} \right], \\ \beta_2 = \frac{1}{2L}\left[\left(L^2 + a_1^2 - a_2^2\right) + \sqrt{\left(a_1^2 + a_2^2 - L^2\right)^2 - 4a_1^2 a_2^2} \right]. \end{cases} \tag{11}$$

Thus, from Eq. (9), we can obtain the radius of the two circles after transformation as

$$a_1' = |w(z)|\big|_{z=-a_1} = \left|\frac{-a_1 - \beta_1}{-a_1 - \beta_2}\right| = \frac{(L+a_1)^2 - a_2^2 - \sqrt{\left(a_1^2 + a_2^2 - L^2\right)^2 - 4a_1^2 a_2^2}}{(L+a_1)^2 - a_2^2 + \sqrt{\left(a_1^2 + a_2^2 - L^2\right)^2 - 4a_1^2 a_2^2}}, \tag{12a}$$

$$a_2' = |w(z)|\big|_{z=L+a_2} = \left|\frac{L+a_2 - \beta_1}{L+a_2 - \beta_2}\right| = \frac{(L+a_2)^2 - a_1^2 + \sqrt{\left(a_1^2 + a_2^2 - L^2\right)^2 - 4a_1^2 a_2^2}}{(L+a_2)^2 - a_1^2 - \sqrt{\left(a_1^2 + a_2^2 - L^2\right)^2 - 4a_1^2 a_2^2}}, \tag{12b}$$

$$\theta' = \arg(w) = \arg\left(\frac{z-\beta_1}{z-\beta_2}\right) = \arg\left(\frac{r^2 + \beta_1\beta_2 - r(\beta_1+\beta_2)\cos\theta + ir(\beta_1-\beta_2)\sin\theta}{r^2 + \beta_2^2 - 2r\beta_2\cos\theta}\right). \tag{12c}$$

After conformal mapping, the radius of the pipe and the radius of the air core will change, as well as the size and location of the two electrodes, thus the current density on the electrode will not be constant but be a function of position. However, the total current through the electrode and the voltage will remain the same as the original, as shown in Fig. 2. Under this conformal transformation, the Laplacian operator is invariant and, therefore, the problem in the transformed plane can be solved easily using concentric theory.

For the resistance between the two electrodes in eccentric case, we can use the same formula (8),

$$R = R' = \Delta V'/I = \frac{a_1'}{\sigma_w I}\sum_{n=1}^{\infty}\frac{1}{n^2(1-\alpha'^m)}\left[\frac{(p_n'\sin n\theta' - q_n'\cos n\theta')\big|_{\theta_1'}^{\theta_2'}}{\theta_2' - \theta_1'} - \frac{(p_n'\sin n\theta' - q_n'\cos n\theta')\big|_{\theta_3'}^{\theta_4'}}{\theta_4' - \theta_3'}\right], \tag{13}$$

where $\alpha' = (a_2'/a_1')^2$. p_n' and q_n' are the coefficient of Fourier series expansion of the transformed boundary condition $j'(\theta') = \sum_{n=1}^{\infty}[p_n'\cos n\theta' + q_n'\sin n\theta']$, which depends on the current density and the location of the electrodes.

Since the current density on the electrode after conformal mapping is changed with location, so in the simulation, the electrode is divided into M segments and the current density on each segment is assumed to be a constant after conformal mapping. $\theta_{1,m-1}$ and $\theta_{1,m}$ denotes the beginning point and ending point of the mth segment on the first electrode, $\theta_{1,m-1}'$ and $\theta_{1,m}'$ is the phase angle corresponding to $\theta_{1,m-1}$ and $\theta_{1,m}$ after conformal mapping, where $\theta_{1,0} = \theta_1$, $\theta_{1,M} = \theta_2$. For the second electrode, we have the same relationship between the phase angles, $\theta_{2,m-1}$ and $\theta_{2,m}$ denotes the beginning point and ending point of the mth segment on the second electrode, $\theta_{2,m-1}'$ and $\theta_{2,m}'$ is the phase angle corresponding to $\theta_{2,m-1}$ and $\theta_{2,m}$ after conformal mapping, where $\theta_{2,0} = \theta_3$, $\theta_{2,M} = \theta_4$. Therefore, the current density on the two electrodes will be

$$j'(\theta') = \begin{cases} J_1', & \theta' \in [\theta_1', \theta_2'], \\ J_2', & \theta' \in [\theta_3', \theta_4'], \\ 0, & \text{otherwise}, \end{cases} \tag{14}$$
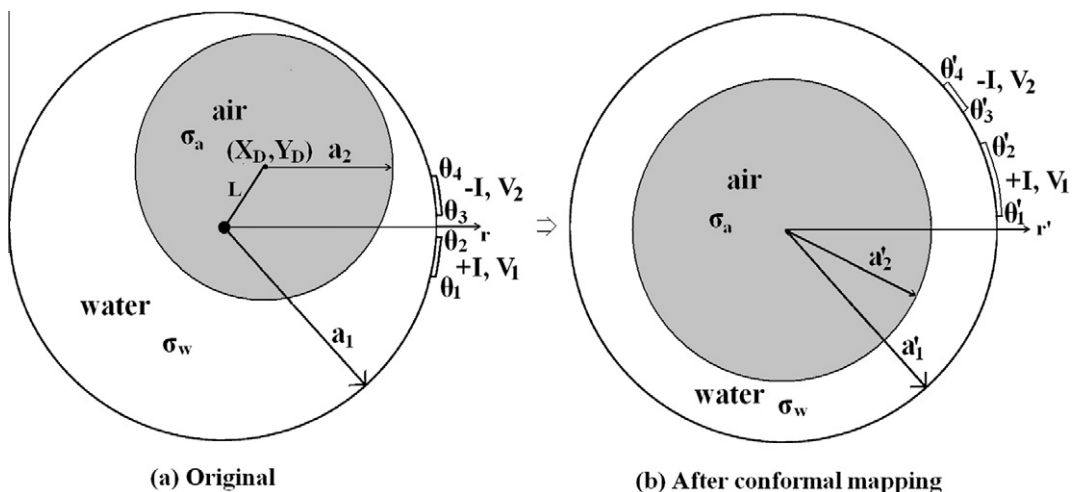
where

Fig. 2. Schematic structure of the annular flow for conformal mapping.

$$J_1' = \frac{Ja_1}{a_1'} \sum_{m=1}^{M} \frac{|\theta_{1,m} - \theta_{1,m-1}|}{|\theta_{1,m}' - \theta_{1,m-1}'|} \left[H\left(\theta' - \frac{\left(\theta_{1,m}' + \theta_{1,m-1}'\right)}{2} + \frac{\left|\theta_{1,m}' - \theta_{1,m-1}'\right|}{2}\right) - H\left(\theta' - \frac{\left(\theta_{1,m}' + \theta_{1,m-1}'\right)}{2} - \frac{\left|\theta_{1,m}' - \theta_{1,m-1}'\right|}{2}\right) \right],$$

$$J_2' = \frac{-Ja_1}{a_1'} \sum_{m=1}^{M} \frac{|\theta_{2,m} - \theta_{2,m-1}|}{|\theta_{2,m}' - \theta_{2,m-1}'|} \left[H\left(\theta' - \frac{\left(\theta_{2,m}' + \theta_{2,m-1}'\right)}{2} + \frac{\left|\theta_{2,m}' - \theta_{2,m-1}'\right|}{2}\right) - H\left(\theta' - \frac{\left(\theta_{2,m}' + \theta_{2,m-1}'\right)}{2} - \frac{\left|\theta_{2,m}' - \theta_{2,m-1}'\right|}{2}\right) \right],$$

and $H(x)$ is the Heaviside function, which is 1 for $x > 0$ and 0 for $x < 0$.

Thus, the Fourier coefficients are

$$p_n' = \sum_{m=1}^{M} \left[\frac{J_1'}{n\pi} \left(\sin n\theta_{1,m}' - \sin n\theta_{1,m-1}' \right) + \frac{J_2'}{n\pi} \left(\sin n\theta_{2,m}' - \sin n\theta_{2,m-1}' \right) \right], \tag{15a}$$

$$q_n' = -\sum_{m=1}^{M} \left[\frac{J_1'}{n\pi} \left(\cos n\theta_{1,m}' - \cos n\theta_{1,m-1}' \right) + \frac{J_2'}{n\pi} \left(\cos n\theta_{2,m}' - \cos n\theta_{2,m-1}' \right) \right]. \tag{15b}$$

3. Numerical results and discussion

For numerical calculations, we set the cross section as a unit circle, i.e. $a_1 = 1$. For the comparison of concentric and eccentric case, we assume that there are 2 electrodes with 0.15 width placed along the boundary of the pipe, and the gap between the electrodes is 0.046. This electrode set-up allows 32-electrode system. We introduce the normalized resistance R^*, expressed as

$$R^* = (R - R_w)/R_w, \tag{16}$$

where R_w is the resistance for homogenous case when the void fraction α is 0.

In concentric case, if the void fraction is fixed, then the water film thickness is identical along the boundary of the pipe. However, in eccentric case, the thickness of the water film varies with the angle. The thickness will be different according to different measuring points (location of the electrodes) in eccentric case as shown in Fig. 3. The resistance values are calculated using Eq. (8) for concentric cases and Eq. (13) for eccentric cases. 3000 terms of Fourier series expansion and 100 segments on the electrode are used in the numerical calculations.

The resistance values for the given thickness of water film for eccentric cases with the gas core center at $D = (0.125, 0.125)$ are compared with the concentric cases for the corresponding thickness of water film, as shown in Fig. 4. We can see that if the thickness of the water film of eccentric case is similar with the water film thickness of eccentric case, the resistance values for the two cases will be similar. Thus, we can make use of this characteristic to estimate the water film thickness in eccentric case by comparing the resistance value. For the estimation of the water film thickness, 32 measurement points were selected for the given void fraction and location of the air core. Fig. 5 shows some of the estimated results compared with the true boundary of the air core.

RMSE (Root Mean Square Error) is calculated to evaluate the performance of the estimation, which can be defined as

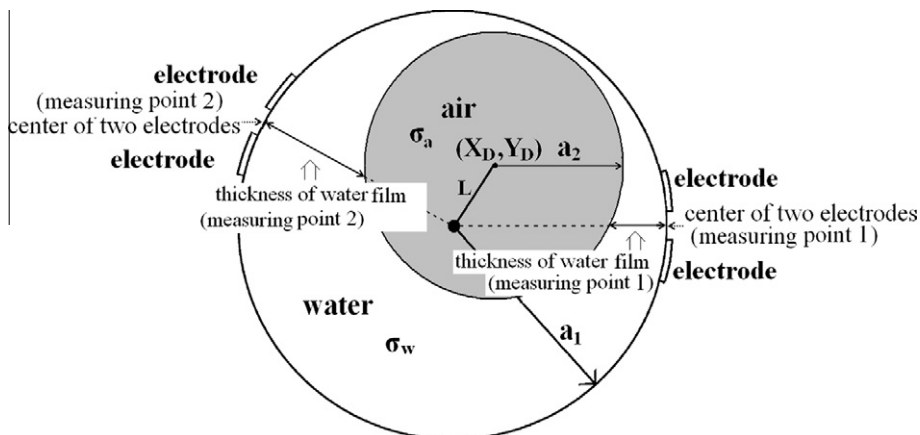$$RMSE = \sqrt{\frac{\sum_{k}^{K} (T_{w,true}(k) - T_{w,estimated}(k))^2}{K}}, \tag{17}$$

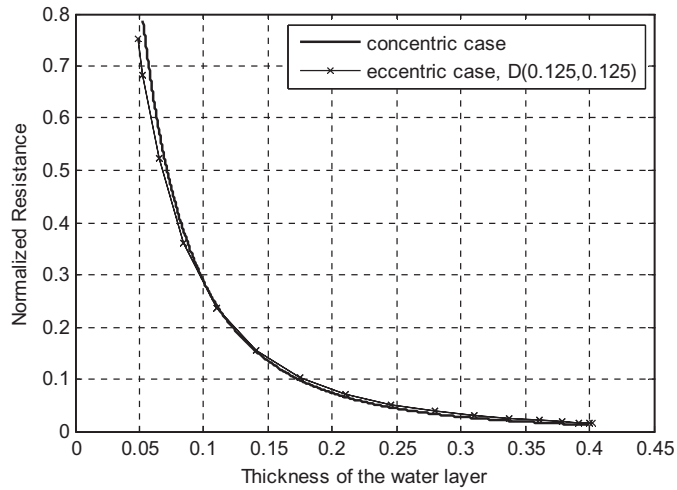**Fig. 3.** Description of the thickness of water film w.r.t. the measuring point.

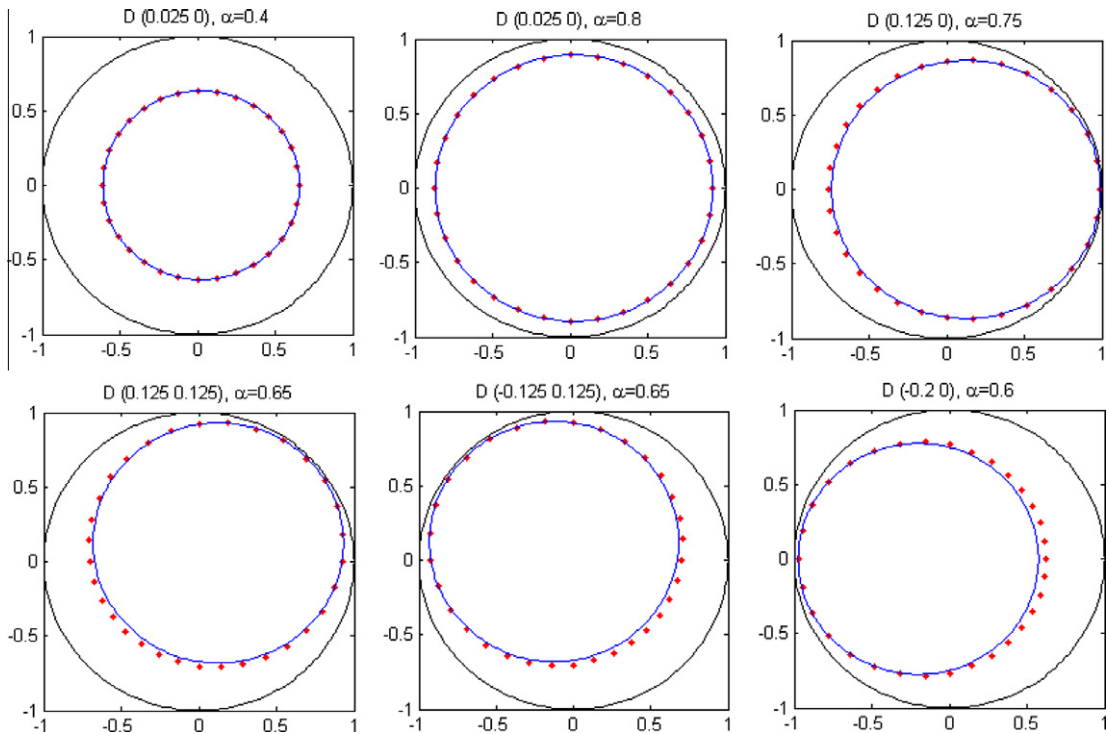**Fig. 4.** Comparison of the resistance values of concentric and eccentric cases.

Fig. 5. Comparison of the estimated location of air core and the true boundary of two-phase annular flow (line: true boundary, dot: estimated points).

where $T_{w,true}$ is the true value of water film thickness and $T_{w,\,estimated}$ is the estimated water film thickness and K is the number of measured points.

Fig. 6 shows the RMSE of film thickness estimates for different cases. It is found that the RMSE increases with the distance of the air core from the center, and it decreases with the void fraction. The film thickness estimation has a good performance when the normalized distance between the gas core center and the pipe center is less than 0.2 and the void fraction is greater than 0.4. The resistance value becomes very small when the water film thickness is greater than 0.4 and this leads a bigger RMSE values as the distance of the air core from the pipe centre increases, However, it should be noted that the annular flow is observed at high void fraction region ($\alpha > 0.7$) and the proposed measurement procedure is fairly applicable to estimation of the liquid film thickness in annular flows.
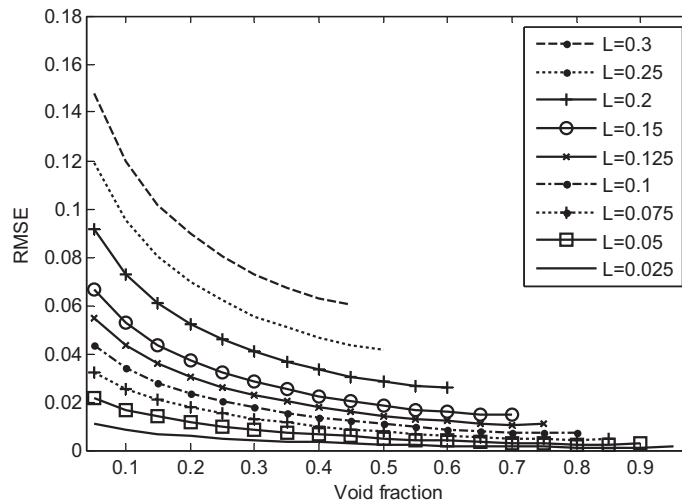
Fig. 6. RMSE of film thickness estimates (*L* is the distance of the air core center from the pipe center).

4. Conclusions

This work deals with the analytical solution of the potential on the boundary of two-phase annular flow. Conformal mapping is employed to get the analytical solution for eccentric case, and the relationship between the void fraction and the resistance was derived. It is found that if the thickness of the water film of eccentric case is similar with the water film thickness of concentric case, the resistance values for the two cases are close to each other. Thus, we make use of this characteristic to estimate the water film thickness (boundary of the air core) in eccentric case by comparing the resistance values. The estimations shows a good performance (RMSE < 0.04) when the distance of the air core center from the pipe center is less than 0.2 and the void fraction is greater than 0.4.

Acknowledgment

References

[1] N.C.G. Markatos, R. Sala, D.R. Spalding, Flow in an annulus of non-uniform gap, Trans. Inst. Chem. Eng. 56 (1978) 28–35.
[2] N.C.G. Markatos, A. Moult, P.J. Phelps, D.B. Spalding, Calculation of steady, three-dimensional, two-phase flow and heat transfer in steam generations, AICHE Symp. Ser. 1 (1979) 485–502.
[3] N.C.G. Markatos, A. K Singhal, Numerical analysis of one-dimensional, two-phase flow in a vertical cylindrical passage, Adv. Eng. Soft. 4 (1978) (1982) 99–106.
[4] N.C.G. Markatos, Modelling of two-phase transient flow and combustion of granular propellants, Int. J. Multiphase Flow 12 (1986) 913–933.
[5] P. Kostamis, C.W. Richards, N.C.G. Markatos, Numerical simulations of two-phase flows with chemical reaction and radiation, PCH. Physicochem. Hydrodyn. 9 (1987) 219–228.
[6] N.C.G. Markatos, Mathematical modelling on single- and two- phase flow problems in the process industries, Revue de l'Institute Francais du Petrole 48 (1993) 631–662.
[7] L.J. Xu, LA. Xu, Gas/liquid two-phase flow regime identification by ultrasonic tomography, Flow Meas. Instrum. 8 (1997) 145–155.
[8] G. Oddie, H. Shi, L.J. Durlofsky, K. Aziz, B. Pfeffer, J.A. Holmes, Experimental study of two and three phase flows in large diameter inclined pipes, Int. J. Multiphase Flow 29 (2003) 527–558.
[9] C. Tan, F. Dong, M. Wu, Identification of gas/liquid two-phase flow regime through ERT-based measurement and feature extraction, Flow Meas. Instrum. 18 (2007) 255–261.
[10] P.A.B. de Sampaio, J.L.H. Faccini, J. Su, Modelling of stratified gas–liquid two-phase flow in horizontal circular pipes, Int. J. Heat Mass Transfer 51 (2008) 2752–2761.
[11] A. Cioncolini, J.R. Thome, C. Lombardi, Algebraic turbulence modeling in adiabatic gas–liquid annular two-phase flow, Int. J. Multiphase Flow 35 (2009) 580–596.
[12] A. Parvareh, M. Rahimi, A. Alizadehdakhel, A.A. Alsairafi, CFD and ERT investigations on two-phase flow regimes in vertical and horizontal tubes, Int. Commun. Heat Mass Transfer 37 (2010) 304–311.
[13] S.C.M. Yu, C.P. Tso, R. Liew, Analysis of thin film thickness determination in two-phase flow using a multifiber optical sensor, Appl. Math. Model. 20 (1996) 540–548.
[14] D. Schubring, A.C. Ashwood, T.A. Shedd, E.T. Hurlburt, Planar laser-induced fluorescence (PLIF) measurements of liquid film thickness in annular flow. Part I: Methods and data, Int. J. Multiphase Flow 36 (2010) 815–824.
[15] D. Schubring, T.A. Shedd, E.T. Hurlburt, Planar laser-induced fluorescence (PLIF) measurements of liquid film thickness in annular flow. Part II: Analysis and comparison to models, Int. J. Multiphase Flow 36 (2010) 825–835.
[16] D. Schubring, T.A. Shedd, Critical friction factor modeling of horizontal annular base film thickness, Int. J. Multiphase Flow 35 (2009) 389–397.
[17] B.N. Kishore, S. Jayanti, A multidimensional model for annular gas–liquid flow, Chem. Eng. Sci. 59 (2004) 3577–3589.

[18] M.W.E. Coney, The theory and application of conductance probes for the measurement of liquid film thickness in two-phase flow, J. Phys. E: Sci. Instrum. 6 (1973) 903–910.
[19] H.C. Kang, M.H. Kim, The development of a flush-wire probe and calibration method for measuring liquid film thickness, Int. J. Multiphase Flow 18 (1992) 423–437.
[20] T. Fukano, Measurement of time varying thickness of liquid film flowing with high speed gas flow by a constant electric current method (CECM), Nucl. Eng. Des. 184 (1998) 363–377.
[21] J.R. Burns, C. Ramshaw, R.J. Jachuck, Measurement of liquid film thickness and the determination of spin-up radius on a rotating disc using an electrical resistance technique, Chem. Eng. Sci. 58 (2003) 2245–2253.
[22] P. de Jong, K.S. Gabriel, A preliminary study of two-phase annular flow at microgravity: experimental data of film thickness, Int. J. Multiphase Flow 29 (2003) 1203–1220.
[23] G. Conte, B.J. Azzopardi, Film thickness variation about a T-junction, Int. J. Multiphase Flow 29 (2003) 305–328.
[24] G. Geraci, B.J. Azzopardi, H.R.E. van Maanen, Effect of inclination on circumferential film thickness variation in annular gas/liquid flow, Chem. Eng. Sci. 62 (2007) 3032–3042.
[25] Q. Fu, L. Yang, Y. Qu, Measurement of annular liquid film thickness in an open-end swirl injector, Aerospace Sci. Technol. (2010), doi:10.1016/j.ast.2010.06.006.
[26] C.B. Tibiriçá, F.J. do Nascimento, G. Ribatski, Film thickness measurement techniques applied to micro-scale two-phase flow systems, Exp. Therm. Fluid Sci. 34 (2010) 463–473.
[27] H. Haddar, R. Kress, Conformal mapping and impedance tomography, Inverse Probl. 26 (2010) 074002, doi:10.1088/0266-5611/26/7/074002 (18pp).
[28] A. Yilmaz, K.E. Akdŏgan, B. Saka, Application of conformal transformation to elliptic geometry for electric impedance tomography, Med. Eng. Phys. 30 (2008) 144–153.
[29] A. Koksal, B.M. Eyiiboglu, Determination of optimum injected current patterns in electrical impedance tomography, Physiol. Meas. 16 (1995) (pp. A99–AI09).